IOP Publishing Physica Scripta
Phys. Scr. 95 (2020) 034005 (8pp) https://doi.org/10.1088/1402-4896/ab5263

Optical spectroscopy and dielectric properties of phosphate-tellurite glasses

S Polosan[1], A Nitescu and M Secu

National Institute of Materials Physics, Atomistilor no 405 A, 77125 Magurele, Romania

E-mail: silv@infim.ro

Received 22 July 2019, revised 17 October 2019
Accepted for publication 29 October 2019
Published 6 February 2020

Abstract

Tellurium metallic colloids were evidence in the phosphate tellurite glasses obtained by the melt quenching method over 1000 °C. The concentration and subsequent color of these glasses strongly depend on the preparation conditions due to the significant differences among the melting point of the component oxides. The presence of Te metallic colloids was evidenced by the magneto-optical measurements at different temperatures, by the shift of the emissions spectra with the excitation wavelength and the thermoluminescence spectra as a result of recombination between the hole centers, created during x-ray irradiation, with the quasi coupled electrons from the surface of the metallic colloids. The peak position in the absorption spectra of these metallic colloids was modeled based on generalized Mie light scattering theory on these metallic structures, taking into account the size and shape of colloids but also the dielectric constant of the phosphate tellurite glasses in which these colloids are embedded.

Keywords: phosphate-telluite, metallic colloids, magnetic circular dichroism, Mie theory, thermoluminescence

(Some figures may appear in colour only in the online journal)

Introduction

Phosphate-tellurite glasses are now widely used due to the phosphate glass former ability, mainly by melt quenching technique [1–3]. Compositional, these glasses include two interesting oxides, one being a classical network former that is phosphate P_2O_5 group [4, 5]. The other one is TeO_2 that is known as a conditional network former because it is not able to vitrify itself in the melt quenching procedure, but with other oxides forms non-conventional glass matrices [6]. P_2O_5 is known as small cation oxide, where most of the polarizability is derived from the oxide ions [7]. Meanwhile, the large radius of Te^{4+} in the oxides (0.84 Å) induces a higher refractive index compared with other glass formers like silicates, borates, phosphates and germanates [8–10]. However, in P_2O_5–TeO_2 glasses, some heteroatomic P–O–Te linkages are observed at lower concentrations of TeO_2, below 1% wt [11]. It has been observed that TeO_4 trigonal bipyramids are transformed in trigonal pyramids when the phosphate concentration increases. This fact was interpreted as an increase of the non-bridging oxygen concentration.

In the case of the P_2O_5–TeO_2–ZnO glasses, the presence of the zinc oxide in the melt quenching obtained below 1300 °C, is considered as an intermediate oxide glass component [12] due to the higher melting point, around 2000 °C [13]. It is reasonable to assume that ZnO acts as a network former which bridges between the PO_4 and TeO_4 chains so that the glass transition temperature increases with the increasing ZnO content [14].

Considering the 340 °C as the melting point of P_2O_5 [15] and 730 °C as the melting point of TeO_2 [16], the melt quenching procedure requires some precautions. Depending on the method of preparation and melt quenching parameters, the phosphate-tellurite glasses are more or less red colored [17]. The origin of this color is connected with the presence of tellurium element which influences the mechanical properties from brittle to a rigid structure of phosphate-tellurite glasses.

In the case of P_2O_5–ZnO glasses, these are colorless having a transparency up to 6 eV, so that the red coloring of P_2O_5–TeO_2–ZnO, could be assigned to the tellurium. Generally, the glass coloration is usually induced by the presence

[1] Author to whom any correspondence should be addressed.

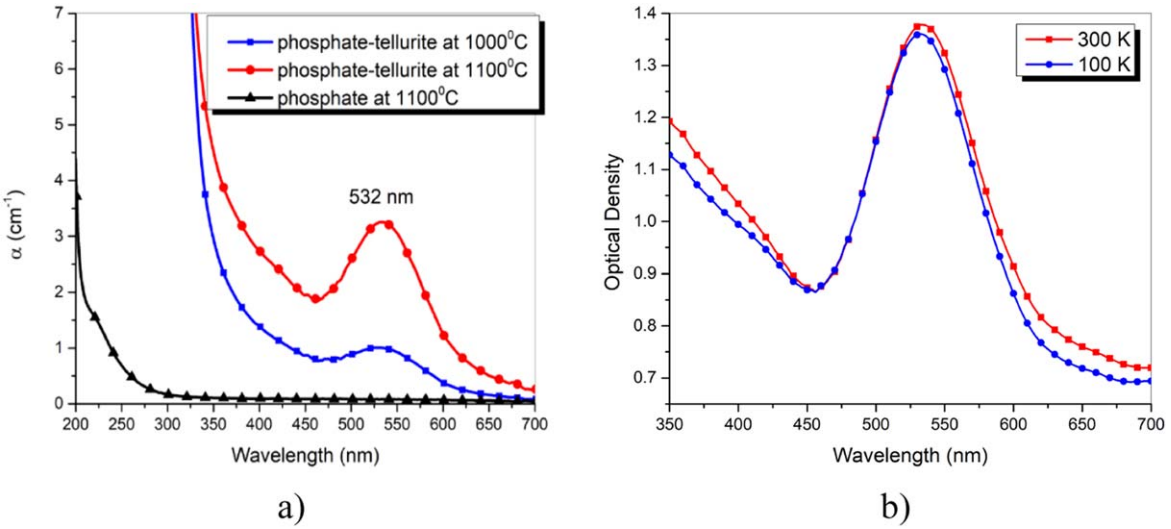

Figure 1. (a) Absorption spectra of 40%ZnO + 40%P_2O_5 + 20%TeO_2 at two melting temperatures and 50%ZnO + 50%P_2O_5 at 1100 °C; (b) temperature dependence of the absorption.

of rare-earth ions, transition metal ions or colloidal suspension as dopants. However, dissolving ions hardly exhibit yellow to red colors in glass materials [18]. The melt quenching temperature is a key parameter because these glasses are usually melted from 1000 °C to 1300 °C and the phase diagram of Te–O shows that 988 °C is the boiling point of tellurium where the solubility of oxygen is very small [19].

In this manuscript, the 40%ZnO + 40%P_2O_5 + 20%TeO_2 glasses, obtained by the melt quenching method, are analyzed both from the experimental and theoretical point of view as a fitting procedure, to explain the red color of these phosphate-tellurite glasses. The parameters of these glasses, like the dimension of tellurium clusters and dielectric constant of glasses, are discussed to identify the origin of the coloring process.

Experimental

Glasses of 20%TeO_2 + 40%ZnO_2 + 40%P_2O_5 and 50%ZnO + 50%P_2O_5 (10 g) were prepared by conventional melt quenching technique by using high purity chemicals of TeO_2 (99.9% purity, Merck Company), ZnO (99.99% purity, Alfa Aesar Company) and P_2O_5 (99% purity, pro analysis Merck Company). The phosphate pentoxide was kept at 100 °C for 1 h before weighing. The chemicals were weighed and set intro alumina (Al_2O_3) crucible starting with P_2O_5, followed by TeO_2 and ZnO, to avoid the evaporation of components due to their different melting points. The crucible was covered with a lid and thermally annealed with 6 °C min^{-1} below the glass transition point (around 400 °C) and then with up to 1100 °C with 3 °C min^{-1}. After 30 min at 1100 °C, the melt was poured in cylindrical graphite crucible preheated at 550 °C–600 °C. The melt was then natural quenched at room temperature (RT) but covered with a lid.

The absorption and magnetic circular dichroism (MCD) were performed on Jasco 815 spectrometer by using a 1.5 Tesla magnet and a Janis cryostat at temperatures from 100 to 300 K. The photoluminescence were recorded by using two LEDs diodes with the emitting wavelengths at 640 and 808 nm and the sample was mounted in an integrating sphere connected with an Ocean Optics FL 2000 spectrofluorimeter by optical fiber and recorded on PC.

Thermoluminescence (TL) measurements were performed on glass samples by using a Harshaw 3500 TL reader, in the range 50 °C–350 °C with a heating rate of 10 °C s^{-1}. Before the TL measurements, the samples were x-rays irradiated at RT at 40 kV and 40 mA for 30 min.

The XRD measurements were performed on a BRUKER D8 ADVANCE type x-ray diffractometer (Karlsruhe, Germany), in focusing geometry, equipped with copper target x-ray tube and LynxEye one dimensional detector, using CuKα1 radiation (1.540 56 Å), at 40 kV and 40 mA. The 2θ scan range was 5–20°, with a step size of 0.02° and a resolution of 0.01°. The line width was determined after subtraction of Ka2 lines from the Ka1–Ka2 doublet, using the Rachinger algorithm with the Bruker Difracplus Basic Evaluation program package. A Zeiss EVO 50 scanning electron microscopy (SEM) with LaB6 cathode with Brucker energy dispersive x-ray (EDX) system was employed for the surface images and compositional analysis of the phosphate-tellurite glasses.

Results and discussions

Optical spectroscopy

The optical properties of the phosphate-tellurite glasses are dependent on the melt quenching procedure. Figure 1(a) presents the absorption spectra of 50%P_2O_5–50%ZnO and 40%P_2O_5–40%ZnO–20%TeO_2. The samples without TeO_2 are transparent up to 200 nm (6.2 eV), while the samples with TeO_2 present two main absorption bands at 532 and 430 nm. The absorption band from 532 nm decreases with the melt

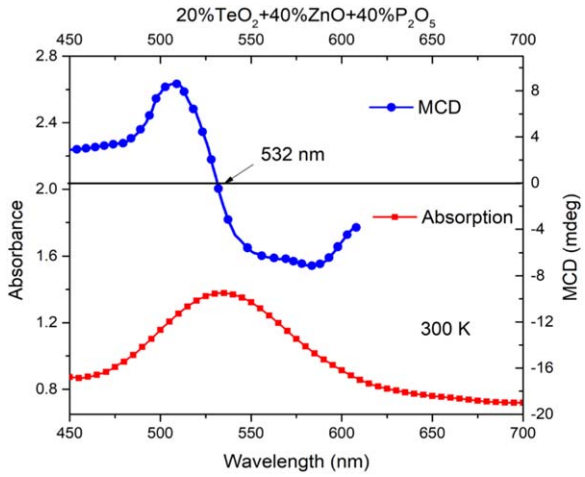

Figure 2. Absorption and MCD spectra recorded at 300 K.

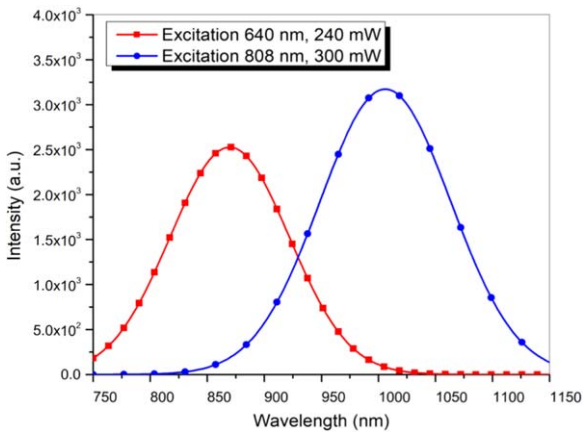

Figure 3. Photo luminescent spectra excited at two wavelengths.

quenching temperature at the same concentration of TeO_2. As can be seen in figure 1(b), the absorption peak from 532 nm (2.33 eV) seems to be formed from two components. One of them, at higher energy, which does not vary with the temperature between 100 to 300 K and one component at lower energy edge which vary with the temperature, increase during absorption measurements.

More than that, this absorption band is considerably reduced when the melting temperature decreases from 1100 °C to 1000 °C. This fact is accompanied by a changing of color from deep purple to purplish red.

To clarify this aspect, MCD measurements, from 80 to 300 K, were performed, in the magnetic field of 1.5 Tesla. The MCD signal gives the difference between the left and right circularly polarized light, more precisely between the optical densities or absorbances of the polarized components of light. The optical densities difference between the left and right circularly polarized lights for an absorption band can be written as [20]:

$$\Delta D = \left(A\frac{\partial f(E)}{\partial E} + \left(B + \frac{C}{kT}\right) * f(E)\right) * H, \qquad (1)$$

where *f(E)* is the shape function of the absorption band and *H* is the applied magnetic field. These three terms are connected with the degeneracy lifting of the ground state and excited states, with changes of the populations via Boltzmann distributions or mixing of the electronic levels. The first *A* term is connected to the diamagnetic properties of the ions being due to the Zeeman splitting of the electronic levels in the magnetic field. The *B* term is connected to the mixing of the electronic levels in the magnetic field and the *C* term is temperature dependent being responsible to the paramagnetic centers.

In figure 2, the absorption spectrum of the $40\%P_2O_5$–$40\%ZnO$–$20\%TeO_2$ is compared with the MCD spectrum at 300 K. As can be seen, an asymmetric S-type MCD spectrum is centered at 532 nm as in the case of the absorption peak, being associated with the localized surface plasmon resonance of metallic nanoparticles. The MCD spectrum shows a pronounced Zeeman splitting which is explained by a substantial enhancement of the magnetic Lorentz force. The collective movement of the conduction electrons induces this force when the localized surface plasmon resonance of the metallic colloids was optically excited. The asymmetry of the S-shape signal indicates a magneto-optical effect that does not originate from a transition to a single degenerate excited state. A careful deconvolution of both absorption and MCD signal suggests the existence of a second band at lower energies, in agreement with the observed absorption spectra at different temperatures. This fact can be explained by a strong intermixing of the excited spin–orbit state, resulting in a negative *B*-term in the MCD signal.

Metallic tellurium Te^0 has an electronic structure like [Kr] $4d^{10}5s^25p^4$ having the ground state term $^3P_2$, while the first excited states being $^3P_1$ and ^3P_o. The absorption spectrum is dominated by the $^3P_2 \rightarrow {}^3P_1$ and $^3P_2 \rightarrow {}^3P_o$ superimposed transitions, which can be easily identified in the MCD as the splitting of the $^3P_1$ state. The $J = 0$ term (*A*-term) marks the center of the absorption while the $J = -1$ and $J = 1$ terms give the positive and negative contributions of $^3P_1$ state to the MCD spectrum accordingly with the Zeeman splitting. The *B*-term is situated at lower energy (580 nm, 2.14 eV) and has a negative sign. Consecutively, the emission bands are shifted towards lower energies due to the $^3P_o \rightarrow {}^3P_2$ transitions and the Stokes shift is around 0.5 eV.

The optical absorption and MCD spectra do not vary in comparison with other metallic colloids, like silver or gold metallic colloids [21–27]. The magneto-optical activity of the metallic colloids is connected with the ability of the surface plasmons of these colloids to localize the electromagnetic field in a very small volume triggering the magneto-optical response in composite nanostructures made out of metals [28]. The absorption peak from 532 nm is assigned to tellurium colloids, which color these glasses, and comes from Mie scattering on the localized plasmon metallic colloids [29, 30].

Figure 3 shows the emission spectra of the $40\%P_2O_5$ $-40\%ZnO$–$20\%TeO_2$ glass sample excited with two LED with light emissions at 640 and 808 nm when the sample was fixed in the integration sphere. Two broad emission peaks

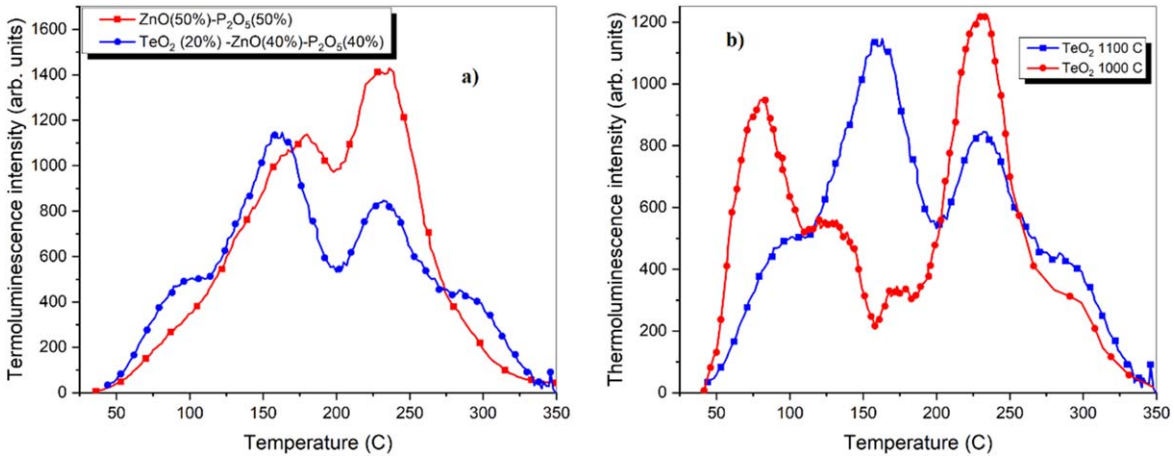

Figure 4. (a) Thermoluminescence of 40%ZnO + 40%P_2O_5 + 20%TeO_2 and 50%ZnO + 50%P_2O_5 melted at 1100 °C; (b) thermoluminescence of 40%ZnO + 40%P_2O_5 + 20%TeO_2 at two melting temperatures.

appear at 850 nm and 1020 nm with a full width at half maximum about 150 nm are observed.

The redshift of the emission peaks with increasing the excitation wavelength was observed in other metallic colloids [31, 32] and was explained by the broadening of the energy levels with the clustering process of the metal. The emission of metallic colloids dependence by the excitation light indicates a strong coupling effect between the surface plasmons and the emitter. A similar result was observed in 50%ZnO–10%TeO_2–50%P_2O_5 glasses by Chen *et al* [33].

TL measurements

Figure 4(a) shows the TL of the 20%TeO_2 + 40%ZnO_2 + 40%P_2O_5 and 50%ZnO + 50%P_2O_5 glass samples irradiated with x-ray, 40 kV and 40 mA for 30 min. In figure 4(b), a comparison between 20%TeO_2 + 40%ZnO_2 + 40%P_2O_5 melted at 1100 °C and the one with the same composition melted at 1000 °C, is done to underline the effect of tellurium concentration in the sample. A strong peak at 282 °C (555 K) is observed in the 20%TeO_2 + 40%ZnO_2 + 40%P_2O_5, which is missing in the sample without TeO_2. This band slightly decreases when the concentration of TeO_2 is reduced. The TL spectrum of 20%TeO_2 + 40%ZnO_2 + 40%P_2O_5 obtained at 1100 °C was deconvoluted and the peak from 282 °C has energy around 1.14 eV and 1.03 eV in the case of 20%TeO_2 + 40%ZnO_2 + 40%P_2O_5 glass sample obtained at 1000 °C.

The band from 282 °C (555 K) was observed in alkali halide crystals irradiated with gamma-rays and was assigned to the colloidal centers [34]. In the case of NaCl crystals, this band appears in the heavily irradiated sample were the sodium metallic nanoparticles are formed. This band was also observed in NaCl:Cu crystals and irradiated with a ^{60}Co source [35]. This band appears due to the recombination between the electrons from the surface of the metallic colloids and the hole centers, produced during irradiation. This TL band has an anomalous shape because it cannot be correlated with the model of the mobile electrons [34]. It was suggested that the dependence of the TL peak position with the size of metallic colloids results in a slight shift of the peak position, which is quite true when the concentration of metallic tellurium colloids increases.

Structural analysis

After the melt quenching procedure, the sample containing TeO_2 is red colored and more stable mechanically (figure 5(b)), while the 50%ZnO + 50%P_2O_5 sample is brittle and transparent in the visible range of the spectrum (figure 5(a)).

The obtained glass samples were milled and investigated through the x-ray diffraction for both compositions 40%ZnO + 40%P_2O_5 + 20%TeO_2 and 50%ZnO + 50%P_2O_5. The peaks in undoped sample are assigned to the orthorhombic structure of phosphorus pentoxide with the following parameters: $a = 9.65$, $b = 9.94$, $c = 7.38$, $\alpha = \beta = \gamma = 90°$ [36].

Because the phosphorus pentoxide is highly hygroscopic, the 50%ZnO + 50%P_2O_5 samples are unstable in the time, leading to a white powder on the sample surface, while the 40%ZnO + 40%P_2O_5 + 20%TeO_2 is more stable, the patterns being recorded after 10 months. In figure 6, the 50%ZnO + 50%P_2O_5 spectrum was arbitrary shifted for a better view.

The SEM images show only a smooth surface of the tellurite glass, while the EDX spectroscopy gives the elemental analysis of this sample (figure 7 and table 1).

In the case of phosphate-tellurite glasses, the ratio 1:2:2 (more precisely 1.35:2.48:2.83) between tellurium, zinc, and phosphor suggests a nominal composition of the initial mixture used before melting procedure. The elemental compositions were obtained in atomic weight percentage, which confirms the formation of the 20%TeO_2 + 40%ZnO + 40%P_2O_5 glass.

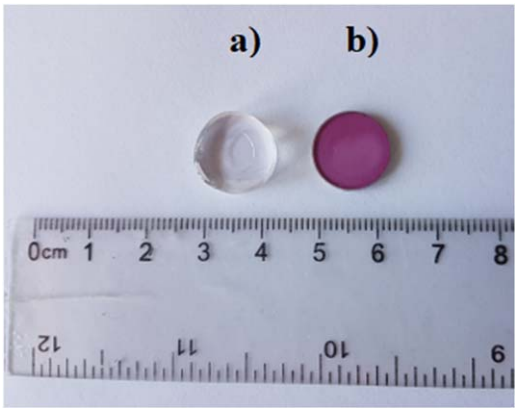

Figure 5. Images of the cut and polished glass samples.

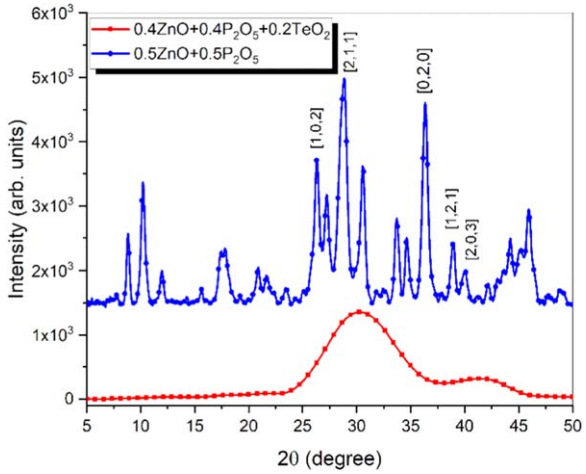

Figure 6. X-ray patterns of 40%ZnO + 40%P_2O_5 + 20%TeO_2 and 50%ZnO + 50%P_2O_5.

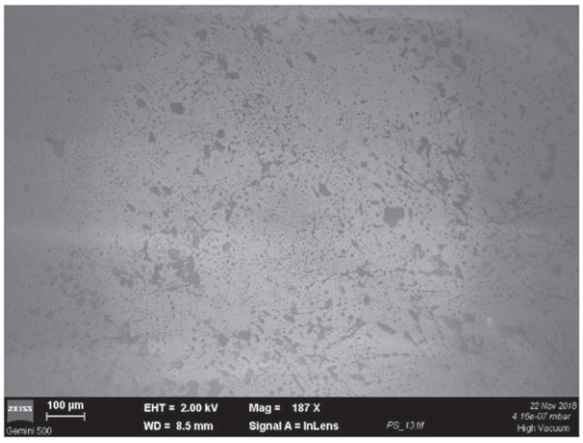

Figure 7. SEM image of tellurite glass sample.

Table 1. EDX analysis of tellurite glass sample.

Elem.	At No	Netto	Mass (%)	At (%)	Err (%)
O	8	142 634	19.59	56.43	6.26
Zn	30	51 378	3.53	2.48	0.72
Te	52	4503	3.74	1.35	0.45
P	15	24 297	1.90	2.83	0.29

Fitting procedure based on Mie theory

The light scattering on the metallic nanoparticles with physical dimensions below the wavelength of the light (below 500 nm) is described by the Mie theory [29]. The theoretical treatment of localized surface plasmons resonance which can be optically excited is based on Maxwell's equations. Briefly, considering a spherical particle with R-radius that is optically excited with a λ wavelength light (with $R/\lambda < 0.1$), the resulting solution for the EM field outside the particle gives an extinction coefficient of the metal sphere:

$$\alpha(\lambda) = \frac{24\pi N R^3 \varepsilon_{\text{out}}^{1.5}}{\lambda \ln(10)} \left[\frac{\varepsilon_{\text{i}}(\lambda)}{(\varepsilon_{\text{r}}(\lambda) + \chi\varepsilon_{\text{out}})^2 + \varepsilon_{\text{i}(\lambda)}^2} \right], \qquad (2)$$

where ε_{r} and ε_{i} are the real and imaginary parts of the metal–dielectric function, N is the concentration (number of particles) of metallic colloids, ε_{out} is the dielectric constants of the environment around the metallic particles and χ is a constant which depends on the shape on colloids [37]. This factor χ is 2 for spherical particles but could be 20 for lower symmetries [38].

For the fitting procedure, the above formula was simplified and introduced in WinMathCad in the following form:

$$\alpha_k = \frac{24\pi^3 \varepsilon_{\text{out}}^{3/2}}{3} N \frac{R^3}{\lambda_k} \frac{\varepsilon_{ik}}{(\varepsilon_{rk} + \chi\varepsilon_{\text{out}})^2 + \varepsilon_{rk}^2}, \qquad (3)$$

where α_k—is the extinction coefficient and k-counts the wavelength dependences of each parameter. The fitting parameters are $N = 10^{19}$ particles, χ taken between 2 and 20, $\varepsilon_{\text{out}} = 12.5$, calculated based on the medium approximation (see below) and the real and imaginary part (ε_{r} and ε_{i}) obtained from the polarized reflectance measurements. These values were compared for both orientations of tellurium nanowires arranged parallel and perpendicular to the electromagnetic field. The mean colloids radius was varied between 2 and 200 nm.

From the above formula, it is clear that the maximum extinction is obtained when the dielectric constant of the metal is roughly equal with $-\chi\ \varepsilon_{\text{out}}$, i.e. the electromagnetic field is enhanced relative to the incident field. The metallic colloids that possess a negative real part dependence of the light wavelength and small positive imaginary dielectric part are capable of supporting the localized surface plasmon resonance. This resonance is seen as a coherent oscillation of the surface conduction electrons optically excited by the light.

In the case of metallic tellurium colloids, these dependencies are shown in figure 8.

In the case of metallic tellurium colloids, the Tutihasi *et al* describe these dependencies [39]. The real part ε_{r} dielectric constant is negative for both parallel and perpendicular direction of light with these metallic nanoparticles, from 300 up to 575 nm, but this negativity has small values (−12) compared with the positive values (figure 8). The imaginary part ε_{i} dielectric constant is always positive for the visible spectrum. These values were taken from the reflectivity measurements that are made in the polarized light on a tellurium single-crystal [39].

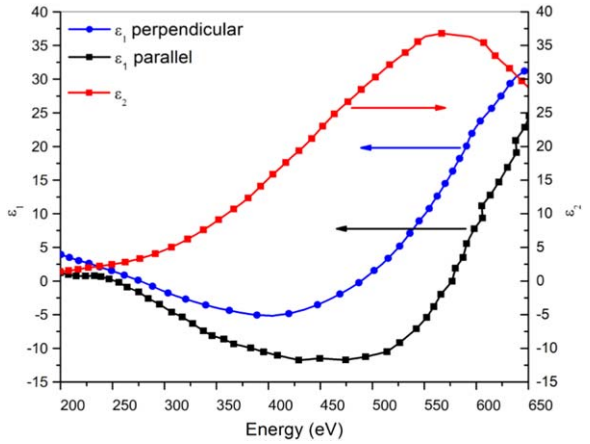

Figure 8. Dielectric constants of tellurium single crystal.

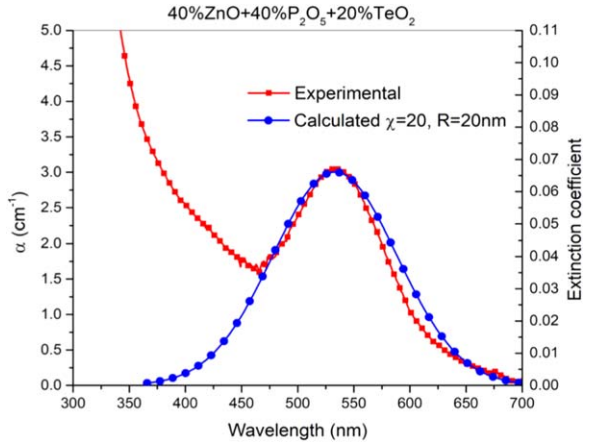

Figure 9. Absorption spectrum compared with the calculated extinction based on Mie theory.

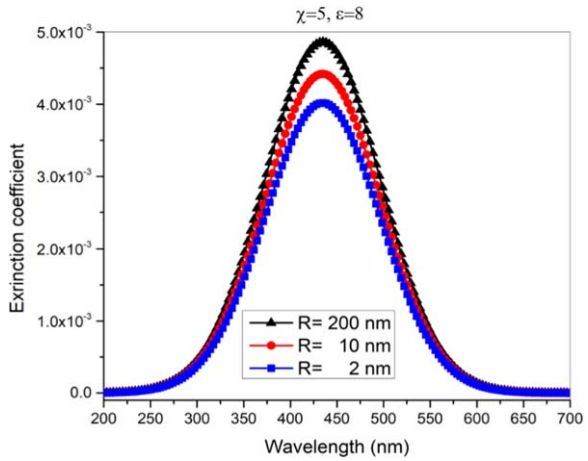

Figure 10. Dependence of the metallic colloid size on the extinction spectra.

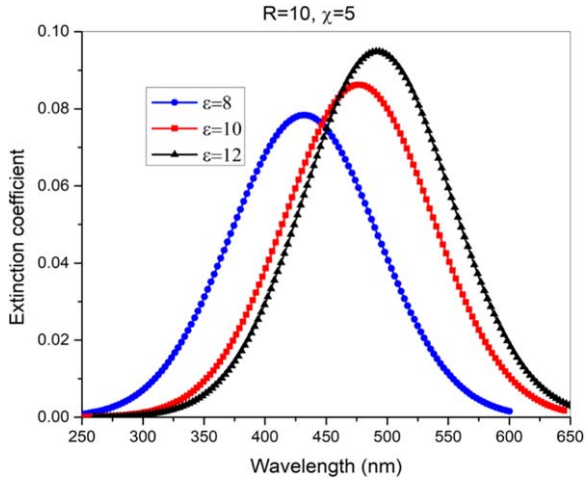

Figure 11. Dependence of the extinction spectra by the dielectric constant of the glass.

The reflectivity measurements were performed on cleaved (1010) surfaces and the dielectric constants were measured with electric vector *E* parallel and perpendicular with the *c*-axis of the tellurite crystal. Tellurium crystal is a semiconductor that has D_3 point group symmetry and is optically uniaxial [40].

Using these values, the extinction coefficient of tellurium colloids was computed with Win Mathcad software and superimposed on the absorption spectrum, adjusting the concentration of colloids to fit the experimental curve (figure 9). The calculated extinction versus the wavelengths is given for a dielectric constant of 12.5 and a shape factor of 20 which were explained below.

Because the real part of the dielectric function of tellurium metal does not significantly vary with the light wavelength, the extinction peak does not vary with the dimension of the tellurium metallic colloids and this fact is presented in figure 10. As can be seen, the peak position is in the same position for a colloidal dimension from 2 up to 200 nm.

The second factor that affects the peak position is the dielectric constant of the $20\%TeO_2 + 40\%ZnO_2 + 40\%P_2O_5$ glass sample (figure 11).

The dielectric constant of glass is derived from the effective value of the total mixture by the effective medium approximation as given by [41]:

$$\varepsilon_{out} = f(TeO_2) * \varepsilon(TeO_2) + f(ZnO) * \varepsilon(ZnO) + f(P_2O_5) * \varepsilon(P_2O_5), \quad (4)$$

where *f*—is the molar fraction and ε—is the dielectric constant of oxides from the sample.

The dielectric constants for each oxide are 25.3 for the α-TeO_2 [42, 43], 14.4 for the ZnO [44] and 4 for the P_2O_5 [45]. Following the nominal composition of our glass $20\%TeO_2 + 40\%ZnO_2 + 40\%P_2O_5$, the medium dielectric constant is around 12.5. This value could slightly vary in the obtained glass due to the large differences between the melting point of each oxide which could induce the evaporation effect and taking into account that a small part (around 14%) from the TeO_2 is converted in Te metallic colloids. The 14% value was obtained from the x-ray photoelectron spectroscopy. The third factor that affects the peak position is the shape factor, which is a ratio between the lengths divided by the width of the tellurium metallic colloid. The calculated peak position was obtained for a maximal value of 20 (figure 12).

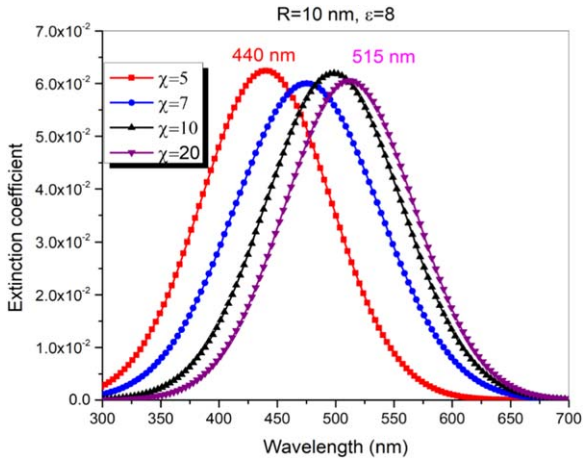

Figure 12. Dependence of the metallic colloid shape factor on the extinction spectra.

This is quite reasonable, because the metallic tellurium structures could tend to form nanorods with a medium width of 17 nm and a medium length of 300 nm, but could also achieve 1000 nm [46].

Conclusions

Phosphate-tellurite glasses with the nominal composition $20\%TeO_2 + 40\%ZnO_2 + 40\%P_2O_5$ and melted at temperatures over 1000 °C, change their color from purplish red to deep purple due to the gradual transformation of TeO_2 in Te metallic colloids. The coloring process is dependent on the time of annealing up to the melting point due to the large differences between the melting points of the three oxides. The presence of colloids is marked by a prominent peak in the visible part of the absorption spectrum, centered at 532 nm (2.33 eV) and an *A*-term with an asymmetric shape, generated by localized surface plasmon resonance specific for metallic colloids. The luminescent peak position of these colloids varies with the excitation wavelength and was explained by the broadening of the energy levels with the clustering process of the metal. The TL patterns of the x-ray irradiated samples reveal a recombination process between the hole centers produced during irradiation with the quasi coupled electrons from the surface of metallic colloids. The absorption peak was fitted based on Mie theory, which allows the calculation of the extinction coefficients. The parameters of the simulated extinction curve depend on the size and shape of the metallic colloids and the dielectric constant of metallic tellurium.

Acknowledgments

This work was supported by a grant of the Romanian Ministry of Research and Innovation, CCCDI-UEFISCI, project number PN III-PI-1.2-PCCDI-2017-0871 within PNCDI III.

ORCID iDs

S Polosan https://orcid.org/0000-0003-3359-8531
M Secu https://orcid.org/0000-0002-8462-7905

References

[1] Lakshminarayana G, Kaky K M, Baki S O, Lira A, Nayar P, Kityk I V and Mahdi M A 2017 Physical, structural, thermal, and optical spectroscopy studies of TeO_2–B_2O_3–MoO_3–ZnO–R_2O (R = Li, Na, and K)/MO (M = Mg, Ca, and Pb) glasses *J. Alloys Compd.* **690** 799–816
[2] Manzani D, Souza J B, Reyna A S, Silva Neto M L, Bautista J E Q, Ribeiro S J L and de Araújo C B 2019 Phosphotellurite glass and glass-ceramics with high TeO_2 contents: thermal, structural and optical properties *Dalton Trans.* **48** 6261–72
[3] Elkhoshkhany N, Mahmoud M and Yousef E S 2019 Structural, thermal, and optical properties of novel oxyfluorotelluride glasses *Chalcogenide Lett.* **16** 265–82
[4] Sardarpasha K R, Hanumantharaju N and Gowda V C V 2018 Optical absorption spectra and energy band gap in manganese containing sodium zinc phosphate glasses *AIP Conf. Proc.* **1953** 090066
[5] Ivascu C, Gabor A T, Cozar O, Daraban L and Ardelean I 2011 FT-IR, Raman and thermo-luminescence investigation of P_2O_5–BaO–Li_2O glass system *J. Mol. Struct.* **993** 249–53
[6] Zachariasen W H 1932 The atomic arrangement in glass *J. Am. Chem. Soc.* **54** 3841–51
[7] Shanon R D and Fisher R X 2016 Empirical electronic polarizabilities of ions for the prediction and interpretation of refractive indices: oxides and oxysalts *Am. Mineral.* **101** 2288–300
[8] Stanworth J E 1952 Tellurite glasses *Nature* **169** 581–2
[9] Polosan S, Negrea R, Ciobotaru I C, Schinteie G and Kuncser V 2015 Ferromagnetic behaviour of bismuth germanate oxides glass-ceramic materials *J. Alloys Compd.* **623** 192–6
[10] Polosan S and Secu M 2010 X-ray excited luminescence and photoluminescence of $Bi_4(GeO_4)_3$ glass-ceramics *Radiat. Meas.* **45** 409–11
[11] Larink D, Rinke M T and Ecker H 2015 Mixed network former effects in tellurite glass systems: structure/property correlations in the system $(Na_2O)_{1/3}[(2TeO_2)_x(P_2O_5)_{1-x}]_{2/3}$ *J. Phys. Chem.* C **119** 17539–51
[12] Sun K H 1947 Fundamental condition of glass formation *J. Am. Ceram. Soc.* **30** 277–81
[13] Yao T 2001 Zinc oxide *Enciclopedia of Materials: Science and Technology* ed KH J Buschow, R W Cahn, M C Flemings, B Ilschner, E J Kramer, S Mahajan, P Veyssière *et al* (Gemany: Elsevier) pp 9883–7 https://www.sciencedirect.com/science/article/pii/B0080431526017885 9780080431529
[14] Konishi T, Hondo T, Araki T, Nishio K, Tsuchiya T, Matsumoto T, Suehara S, Todoroki S and Inoue S 2003 Investigation of glass formation and color properties in the P_2O_5–TeO_2–ZnO system *J. Non-Cryst. Solids* **324** 58–66
[15] Onodera Y, Kohara S, Masai H, Koreeda A, Okamura S and Ohkubo T 2017 Formation of metallic cation-oxygen network for anomalous thermal expansion coefficients in binary phosphate glass *Nat. Commun.* **8** 15449
[16] El-Mallawany R A H 2002 *Tellurite Glasses Handbook: Physical Properties and Data* (USA: CRC Press) p 12
[17] Du X, Zhang L, Dong G, Sharafudeen K, Wen J, Chen D, Qian Q and Qiu J 2014 Coloration and nonlinear optical

properties of ZnTe quantum dots in ZnO–TeO_2–P_2O_5 Glasses *J. Am. Ceram. Soc.* **97** 185–8
[18] Bamford C R 1977 *Color Generation and Control in Glass* (Amsterdam: Elsevier Scientific Publishing Company) p 88
[19] Itkin V P and Alcock C B 1996 The O-Te (oxygen-tellurium) system *J. Phase Equilib.* **17** 533–8
[20] Stephens P J 1976 Magnetic circular dichroism *Adv. Chem. Phys.* **35** 197–264
[21] Skillman D C and Berry C R 1973 Spectral extinction of colloidal silver *JOSA* **63** 707–13
[22] Zaitoun M A, Roy Mason W and Lin C T 2001 Magnetic circular dichroism spectra for colloidal gold nanoparticles in xerogels at 5.5 K *J. Phys. Chem.* B **105** 6780–4
[23] Modine F A and Orera V M 1981 Magneto-optical properties of metallic colloids in insulators *Phys. Rev.* B **24** 1159–63
[24] Henglein A 1999 Radiolytic preparation of ultrafine colloidal gold particles in aqueous solution: optical spectrum, controlled growth, and some chemical reactions *Langmuir* **15** 6738–44
[25] Suga Y, Nakashima K, Yamauchi N, Yasuda Y, Morita T and Kobayashi Y 2019 Preparation of high-concentration colloid solutions of metallic copper particles and their use in metal–metal bonding processes *SN Appl. Sci.* **1** 925
[26] Shiri M S Z, Henderson W and Mucalo M R 2019 A review of the lesser-studied microemulsion-based synthesis methodologies used for preparing nanoparticle systems of the noble metals, Os, Re, Ir and Rh *Materials* **12** 1896
[27] Ali M and Lin I N 2019 Controlling morphology-structure of gold tiny particles, nanoparticles and particles at different pulse rates and pulse polarity *Adv. Nat. Sci., Nanosci. Nanotechnol.* **10** 1–14
[28] Artemyev M, Krutokhvostov R, Melnikau D, Oleinikov V, Sukhanova A and Nabiev I 2012 Low-field magnetic circular dichroism in silver and gold colloidal nanoparticles of different sizes, shapes, and aggregation states *Proc. SPIE* **8457** 845729
[29] Gafwl M 1908 Beitrage zur Optik truben Medien, speziell kolloidaler metalosungen *Ann. Phys.* **25** 377–445
[30] Vasile E, Datcu M, Polosan S, Apostol E and Topa V 1999 Silver nanocrystals obtained by the ionization of Ag^--ions in KCl *J. Cryst. Growth* **198** 806–10
[31] Chen Y, Yang T, Pan H, Yuan Y, Chen L, Liu M, Zhang K, Zhang S, Wu P and Xu J 2014 Photoemission mechanism of water-soluble silver nanoclusters: ligand-to-metal–metal charge transfer versus strong coupling between surface plasmon and emitters *J. Am. Chem. Soc.* **136** 1686–9
[32] Bellessa J, Bonnand C, Plenet J C and Mugnier J 2004 Strong coupling between surface plasmons and excitons in an organic semiconductor *Phys. Rev. Lett.* **93** 036404
[33] Chen Q, Zhang F, Chen Z and Qiu J 2017 Near-infrared luminescence property of Te-doped zinc phosphate glasses *J. Non-Cryst. Solids* **458** 76–9
[34] Deshmukhs B T, Omanwar K and Moharil S V 1986 Thermolumineseenee of colloidal centres in NaCl *Phys. Status Solidi* a **96** 211–5
[35] Delgado L and Alvarez Rivas J L 1981 Thermoluminescent processes involving Cu^- and F centers in NaCl:Cu irradiated at room temperature *Phys. Rev.* B **23** 6699–710
[36] Persson K 2014 Materials Data on P_2O_5 (SG:62) by Materials Project https://www.osti.gov/biblio/1323146osti.gov
[37] Willets K A and Van Duyne R P 2007 Localized surface plasmon resonance spectroscopy and sensing *Annu. Rev. Phys. Chem.* **58** 267–97
[38] Link S and El-Sayed M A 1999 Spectral properties and relaxation dynamics of surface plasmon electronic oscillations in gold and silver nanodots and nanorods *J. Phys. Chem.* B **103** 8410–26
[39] Tutihasi S, Roberts G G, Keezer R C and Drews R E 1969 Optical properties of tellurium in the fundamental absorption region *Phys. Rev.* **177** 1143–50
[40] Blakemore J S, Long D, Nomura K C and Nussbaum A 1962 *Progress in Semiconductors* (New York: Wiley) 6, 38
[41] Li Y H and Lue J T 2007 Dielectric constants of single-wall carbon nanotubes at various frequencies *J. Nanosci. Nanotechnol.* **7** 3185–8
[42] Li Y, Fan W, Sun H, Cheng X, Li P and Zhao X 2010 Structural, electronic, and optical properties of α, β, and γ-TeO_2 *J. Appl. Phys.* **107** 093506
[43] Thomas P A 1988 The crystal structure and absolute optical chirality of paratellurite, α-TeO_2 *J. Phys. C: Solid State Phys.* **21** 4611–27
[44] Chong E, Hwang S, Sung W, Kim H and Shin H 2009 Dielectric constant and optical reflectance of ceramic filler-added BaO–ZnO–B_2O_3–P_2O_5 glass composites *Int. J. Appl. Ceram. Technol.* **6** 295–301 https://ceramics.onlinelibrary.wiley.com/doi/pdf/10.1111/j.1744-7402.2008.02273.x
[45] https://ceramics.onlinelibrary.wiley.com/doi/pdf/10.1111/j.1744-7402.2008.02273.x
[46] Liu Z, Hu Z, Liang J, Li S, Yang Y, Peng S and Qian Y 2004 Size-controlled synthesis and growth mechanism of monodisperse tellurium nanorods by a surfactant-assisted method *Langmuir* **20** 214–8